








Determination of the dynamic parameters of Speswhite kaolin with resonant column and centrifuge tests

Filipe Cavalcanti Fernandes^{1#} , Bárbara Luiza Riz de Moura² ,
Marcio de Souza Soares de Almeida² , Luciano de Oliveira Souza Junior³ ,
Samuel Felipe Mollepaza Tarazona⁴ , Maria Cascão Ferreira de Almeida⁵ ,
José Maria de Camargo Barros⁶ 

Article

Keywords

Resonant column
Centrifuge models
Dynamic parameters
Soft soil
Speswhite kaolin

Abstract

Understanding the dynamic behavior of soils is essential to the study of the influence of seismic loads on the instability of submarine slopes, an important issue in Brazil and other countries. The shear modulus and the damping ratio are two fundamental parameters for the study of this behavior. Determining these parameters for Speswhite kaolin clay is the object of the present study using resonant column tests and dynamic centrifuge tests with accelerometers and pairs of bender elements. The curves obtained in the laboratory are compared with empirical curves and comparable data in the literature. Good agreement was observed between experimental data and the empirical prediction for the degradation curve of the normalized shear modulus. The damping curve for very low strains, obtained with resonant column tests, was consistent with the empirical curve. However, consistent with a trend observed in the literature, the centrifuge test results presented considerable scatter (dispersion), attributable to the difficulty in modelling damping dissipation mechanisms in the centrifuge.

1. Introduction

The typical geological profiles of submarine slopes on the Brazilian continental margin consist of normally to slightly overconsolidated clays with depths ranging from a few meters to hundreds of meters (Kowsmann et al., 2015). These slopes are often subjected to different types of loading conditions, including dynamic loading, such as earthquakes.

Borges et al. (2020a) observed an important concentration of epicenters in Campos, Santos, and Pelotas basins in southeastern Brazil, along the continental slope. Additionally, topographic surveys have indicated a great concentration of steep seabed slopes in the same area. Due to these unfavorable local conditions, regional earthquakes pose significant risk when they trigger submarine landslides, what could cause major impacts to offshore structures (Mérindol et al., 2022).

Therefore, the evaluation of risk imposed by earthquakes on submarine slopes should include an understanding of local soil behavior under dynamic conditions. Local soil and topographic settings can strongly influence the nature of

vibrations from seismic events, resulting in signal amplification at certain frequencies. The determination of dynamic soil properties, such as shear modulus and damping ratio, is necessary for predicting non-linear stress-strain behavior and for analyzing the stability of geostructures under cyclic loading. Some types of tests can be used to determine the shear wave velocity (V_s) and the maximum shear modulus (G_{max}) of the soil, such as the in situ seismic cone penetration test – *SCPTu* (Borges et al., 2020b) – and the laboratory tests with bender elements and resonant column techniques (Kondner, 1963; Hardin & Drnevich, 1972; Liu et al., 2021; Jafari et al., 2022).

Shear modulus (G) and damping ratio (D) can be obtained employing resonant column (*RC*) tests for a wide range of strains (Atkinson, 2007) with satisfactory control of the test conditions at low strain levels in a range of 10^{-4} to $10^{-1\%}$ (Madhusudhan & Kumar, 2013; Lang et al., 2020).

Instead of *RC* tests, the G_{max} determination corresponding to strains lower than $3 \times 10^{-2\%}$ (Jia, 2018) can be done using bender element (*BE*) testing. The *BE* test enables

#Corresponding author. E-mail address: ffernandes@me.com

¹EFEX Engenharia, Natal, RN, Brasil.

²Universidade Federal do Rio de Janeiro, Instituto Alberto Luiz Coimbra, Rio de Janeiro, RJ, Brasil.

³Klohn Crippen Berger, Belo Horizonte, MG, Brasil.

⁴Vale S.A., Nova Lima, MG, Brasil.

⁵Universidade Federal do Rio de Janeiro, Escola Politécnica, Rio de Janeiro, RJ, Brasil.

⁶Instituto de Pesquisas Tecnológicas, Unidade de Ensino Tecnológico, São Paulo, SP, Brasil.

Submitted on December 3, 2022 ; Final Acceptance on April 1, 2023; Discussion open until August 31, 2023.

<https://doi.org/10.28927/SR.2023.013422>



This is an Open Access article distributed under the terms of the Creative Commons Attribution License, which permits unrestricted use, distribution, and reproduction in any medium, provided the original work is properly cited.

measurement of this parameter for strains below $10^{-3}\%$, a range in which G is almost constant (Mair, 1993; Youn et al., 2008; Wang et al., 2021).

The goal of this study is to present the dynamic geotechnical characterization of Speswhite kaolin which has been used in seismic response studies for submarine slopes (Tarazona et al., 2020; Soriano et al., 2021; Soriano et al., 2022) especially for its high permeability - favorable to centrifuge tests - and for being commercially available. This research uses traditional resonant column tests and centrifuge tests of submerged canyon models instrumented with accelerometers and bender elements to obtain the dynamic parameters of Speswhite kaolin: the moduli, G and G_{max} , and the damping ratio D .

2. Studied soil

Speswhite kaolin (*SK*), a clay of industrial origin, has long been used in geotechnical centrifuges for physical modeling by laboratories around the world (Almeida et al., 1985). The static properties of the *SK* used in this test program was characterized by means of monotonic loading tests (triaxial tests of the *CIU* and *CAU* type, and isotropic consolidation tests) and by index tests such as plastic limit and liquid limit tests. Table 1 presents a summary of the main static properties of the studied material – obtained from Fernandes (2018) – which are in agreement with the literature reports (Al-Tabbaa, 1987; Phillips, 1988; Kutter & James, 1989), where w_L is the liquid limit, I_p the plasticity index, G_s the specific gravity, c_v the coefficient of consolidation, M the critical state friction ratio, λ the slope of the isotropic compression line and κ the slope of the isotropic unload-reload line.

3. Resonant column tests

The preparation of the material for *RC* tests started with the consolidation (to 80 kPa) of a slurry mixture at 1.5 times the liquidity limit to obtain a block of clay from which small samples were extracted. Prior to the *RC* tests, an isotropic consolidation was carried out in a triaxial chamber under a confining stress of 150 kPa, using 5 cm × 15 cm cylindrical samples, to reduce any disturbance due to the transfer of the samples and to guarantee a better consistency of the material for the final molding of the samples (Barros et al., 2007). The final geometry of the samples for the *RC* tests was 3.5 cm in diameter by 8 cm in height.

The *RC* test program was conducted in two phases: (1) the loading phase, or normally consolidated phase, where

each confining stress is the maximum applied stress, and (2) the unloading or overconsolidated phase (overconsolidated ratio, *OCR*, of 2, 4, 7.85 and 15.7).

The *RC* test essentially consists of the application of sinusoidal torsion vibrations, which result in very small shear strains (on the order of 10^{-4} to $10^{-2}\%$) in a cylindrical specimen, previously subjected to a confining stress in a triaxial chamber. The test apparatus presented in Figure 1 is composed of various electronic components (Fernandes, 2018).

A Hall type oscillator (Hall & Richart, 1963) was used in the test in “fixed-free” model, using a rigid mass on top of the specimen for better distribution of strains along the specimen (Richart et al., 1970). The scope of the present study only covers at hydrostatic state of stress.

The oscillator allows a certain stiffness added to one of the ends to add a polar moment of inertia (I_0) at the top

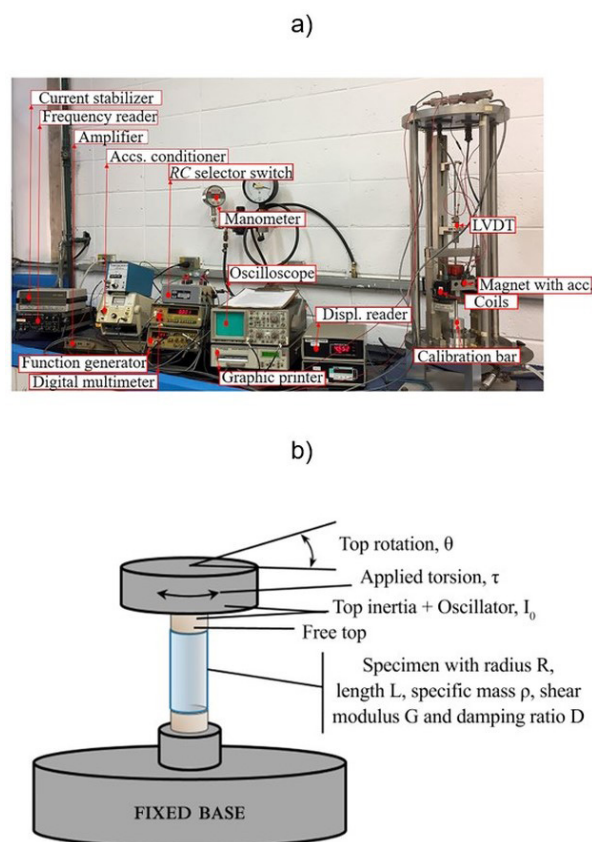


Figure 1. Resonant column test apparatus: a) overview (Adapted from Fernandes, 2018); b) test specimen torsion scheme and variables (adapted from Richart et al., 1970).

Table 1. Main properties of the studied soil (Fernandes, 2018).

Parameter	Parameters of Speswhite kaolin						
	w_L (%)	I_p (%)	G_s	c_v (10^{-8} m ² /s)	M	λ	κ
Fernandes (2018)	62	39	2.615	3.4–34.7	0.93	0.145–0.190	0.039–0.050

of the specimen (Figure 1b). This procedure of applying a torsion (τ) to the “free” end provides an approximately linear variation of angular rotation (θ) along the specimen of radius (R), length (L) and specific weight (ρ), and parameters G and D , thus obtaining a more uniform distribution of the shear strain along the length of the sample (Richart et al., 1970).

The main feature of the Hall-type oscillator is that it does not have a damper system (longitudinal and torsional springs as used in other types of oscillators (Richart et al., 1970)). As proposed by Hall & Richart (1963), the “fixed-free” system coupled to the Hall-type oscillator also enables the determination of the damping ratio (D) by the free-vibration decay method.

3.1 Measurements

The maximum shear modulus (G_{max}) of the soil is measured after 1000 minutes of consolidation. Anderson & Stokoe (1978) disregarded the creep or secondary consolidation effects of consolidation in the sample. Due to a variation in the start time of the tests, sometimes the measurement was not carried out exactly at the instant of 1000 minutes after the beginning of the consolidation stage. Therefore, an interpolation was made based on previous measurements to infer the G_{max} .

In order to determine the G modulus in the resonant condition (ASTM, 2007), measurements of the tangential acceleration of the specimen are performed during the application of vibration (measured by the voltmeter) and vibration frequency (measured directly by the frequency meter). The resonance condition of the system occurs when the signals of the vibration emission frequency and the ground response frequency are in phase. The phase between the torque application signals and the ground response is given by formation of the Lissajous ellipse (ASTM, 2007) on the oscilloscope screen, indicating a lag of 0.5π radians, and the occurrence of resonance in the ground-oscillator system.

In RC tests, the damping ratio can be calculated in more than one way. One of them, standardized by ASTM D4015-07 (ASTM, 2007), involves measuring free vibration decay. Free decay, as presented by Richart et al. (1970), occurs when the function generator is turned off while the amplitude of the accelerometer response is monitored as a function of time (Fernandes, 2018).

4. Centrifuge tests

A series of centrifuge tests were carried out to evaluate the seismic response of submarine slopes and/or canyons, determining the evolution of dynamic soil properties for different earthquake events (Tarazona, 2019; Tarazona et al., 2020, Souza, 2021; Soriano et al., 2021, 2022). The results of these centrifuge tests are useful for the dynamic characterization of the material, complementing the results of RC tests.

The centrifuge tests discussed here were carried out in a submerged clayey model, tested initially in the flat configuration and then as a canyon with a 30° angle. The model made with Speswhite kaolin was consolidated up to a stress of 250 kPa in an ESB (Equivalent Shear Beam) type test box in four successive layers. This level of consolidation stress was chosen to reproduce the undrained shear strength (S_u) profiles observed in the seabed of southeastern Brazil (Soriano et al., 2021). Sensors (such as accelerometers and bender elements) were arranged along its entire depth and were positioned during the consolidation process.

The ESB box was placed on the shaking table and embarked on the centrifuge. The model was then accelerated to 40 times the Earth’s gravity (g) and subjected to two different types of seismic loads, one sinusoidal and the other based on an earthquake that occurred in Italy in 2012 (Emilia Earthquake), applied alternately and with increasing peak ground accelerations (PGA) (Table 2). Additional information on the centrifuge experiments used here can be obtained in Tarazona (2019), Tarazona et al. (2020) and Souza (2021).

Figure 2 shows the final configuration of the centrifuge model with accelerometer sensors A and pairs of bender elements BE and Figure 3 shows one of the inputs applied, the Emilia earthquake, with an amplitude of 0.05g.

The accelerometers enabled the determination of the shear modulus and damping parameters as a function of the strains using the sinusoidal input motion data. The bender elements, in turn, were used to calculate the maximum shear modulus at each excitation stage.

For each configuration of the model, flat F and canyon C , a penetration test was performed using a T-bar (Randolph & Houlsby, 1984) at the beginning of the 40g tests to obtain the profiles of undrained strength S_u and shear wave velocity V_s (Figure 4).

The theoretical S_u profiles were obtained from Equation 1 (Wroth, 1984), also shown in Figure 4a, where K is the normalized strength parameter, σ'_{vo} the effective vertical stress, and m the exponent. The K and m values adopted are shown in Table 3.

$$S_u = K \cdot \sigma'_{vo} \cdot OCR^m \quad (1)$$

Table 2. Input motions applied to the model.

Sequence	Type	PGA
1	Emilia	0.05g
2	Sinusoidal	
3	Emilia	0.075g
4	Sinusoidal	
5	Emilia	0.10g
6	Sinusoidal	
7	Emilia	0.15g
8	Sinusoidal	

Figure 4a shows a clear decrease in strength between the canyon and the flat model up to 4 m depth, showing the effect of the degradation that occurred during the excitation

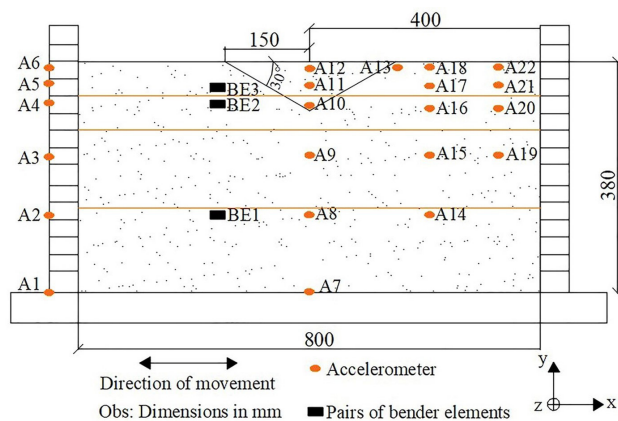
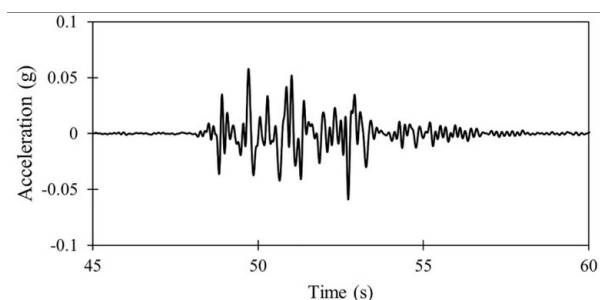
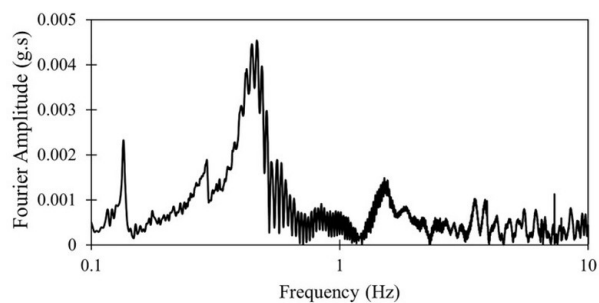


Figure 2. Model configuration and instrumentation.



a)



b)

Figure 3. Emilia input of 0.05g amplitude: a) accelerogram; b) Fourier amplitude.

Table 3. Parameters to calculate theoretical S_u .

Parameter	K	m
Fernandes (2018)	0.234	0.528
Garnier (2001)	0.19	0.59

of the flat model. For greater depths, this effect is not clearly observed.

The OCR profile obtained with Equation 1 from the S_u profile measured by the T-bar was used for the calculation of G_{max} as a function of depth according to Equation 2 (Viggiani & Atkinson, 1995), where p_r is the reference stress (equal to 1 kPa), p' is the mean effective stress and A , n and k are parameters used according to Viggiani & Atkinson (1995).

$$\frac{G_{max}}{p_r} = A \left(\frac{p'}{p_r} \right)^n \cdot OCR^k \quad (2)$$

The V_s profile (Figure 4b) is obtained from Equation 3 using the correlation with the density (ρ) of the model, $\rho = 1.74 \text{ g/cm}^3$ being the average model value used here.

$$V_s = \sqrt{\frac{G_{max}}{\rho}} \quad (3)$$

There was good agreement between the S_u data and the theoretical prediction, especially for the parameters reported by Fernandes (2018). Some humps are present due to the disturbance of the T-bar drive actuator system (Garala & Madabhushi, 2019; Tarazona, 2019 and Zhang et al., 2016). However, discontinuity between layers is not observed. The top of the clay model, up to approximately 1 m, prototype scale, exhibited S_u values higher than expected, possibly due to drying of the surface during model preparation, although care was taken to mitigate this problem such as covering the soil with wet geotextile and plastic.

4.1 Shear modulus and damping through accelerometers

The accelerometers installed in the centrifuge models by Tarazona et al. (2020) were used to obtain the shear modulus and the damping ratio based on the solution proposed by Brennan et al. (2005). In order to determine a value of G and D under a given shear strain (γ), three accelerometers were jointly analyzed at time and the accelerometers at the ends were used to measure the boundary conditions. For this purpose, a filter band of 0.75 Hz to 8.5 Hz was applied to the recorded accelerograms inside in a prototype scale.

Thus, for shear stress and strain histories calculated with the Brennan et al. (2005) formulation, the first 10 stress-strain cycles were individualized – including the first cycle of irregular behavior in blue –, and 10 values of G and D were obtained (Figure 5). Figure 5a shows the 10 hysteresis loops measured with the accelerometer A10 in the 0.15g sine signal and Figure 5b contains only one of the loops with an illustrative scheme for obtaining G (inclination of the highlighted secant line) and D (relative to the demarcated areas) with this method.

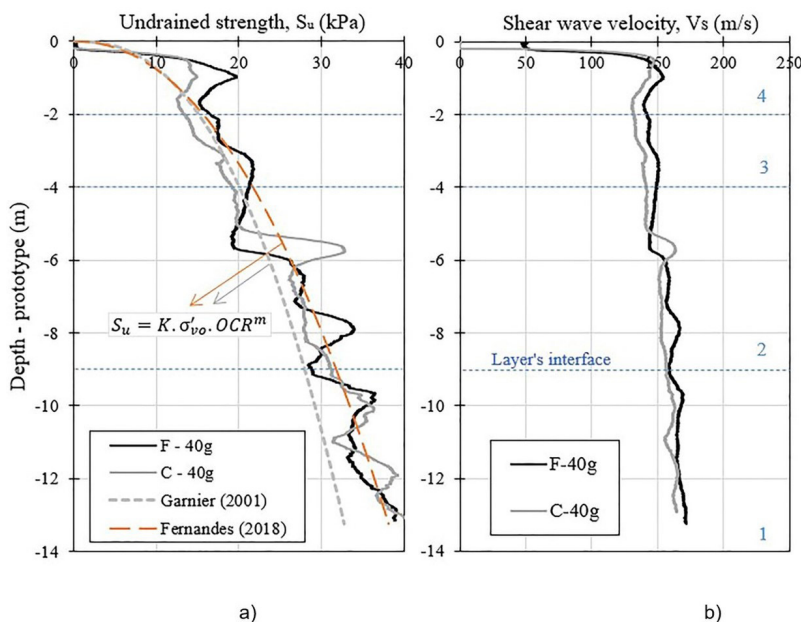


Figure 4. Profiles of a) S_u compared with theoretical predictions and of b) V_s for flat and canyon models.

The G results were obtained from the accelerometers with sine input motions in the flat and 30° canyon models. Results from Tarazona et al. (2020) data are also plotted for comparison.

4.2 Maximum shear modulus from bender element tests

The determination of the maximum shear modulus (G_{max}) was carried out using three pairs of bender elements ($BE1$, $BE2$ and $BE3$ shown in Figure 2). In each pair, one is the transmitter of the wave and the other, the receiver, depending on the arrangement of the cables and the applied polarization (Ingale et al., 2017).

The distance between transmitter and receiver benders (d) and the time interval (t) elapsed between the outgoing and incoming signals are needed for calculating the shear wave velocity V_s . The distance (d) was easily obtained by direct measurement when the sensors were installed in the model, namely: pair $BE1$ is positioned 100 mm apart, $BE2$ is 102 mm and $BE3$ is 108 mm. Ingale et al. (2017) and Lee & Santamarina (2005) present three methodologies for determining time t : in the time domain, in the frequency domain, and by cross-correlation.

In the present study, two methodologies were used to determine the travel time (t) of the shear wave, both in the time domain (TD). The time (t) is the average between two-time intervals used: the first and second peak between the input and output waves, resulting in time intervals t_1 and t_2 , respectively. In the output signal, the points of interest are first observed, and then the first low-amplitude inflection wave is disregarded (Lee & Santamarina, 2005). Figure 6 schematically

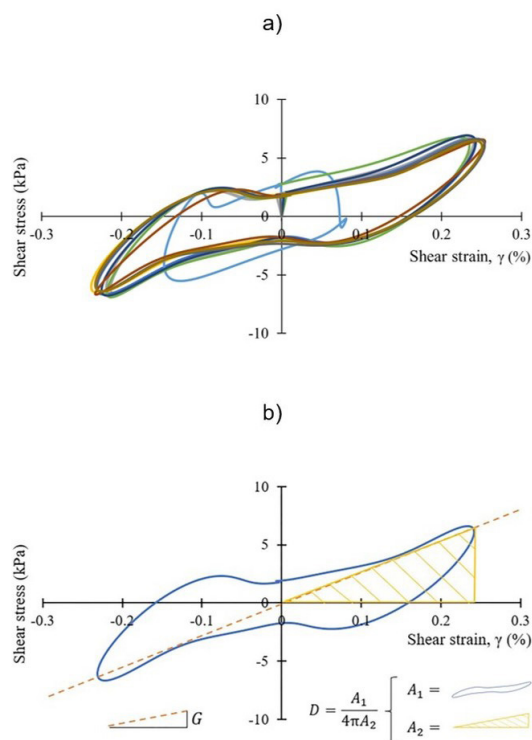


Figure 5. Linear equivalent solution of G and D : a) ten hysteresis loops for the 0.15g sine input motion (at A10); b) scheme for obtaining G and D .

summarizes the methodology used to obtain the intervals t_1 and t_2 for a sample of waves observed in pair $BE3$ after the 0.15g sinusoidal input motion (flat model).

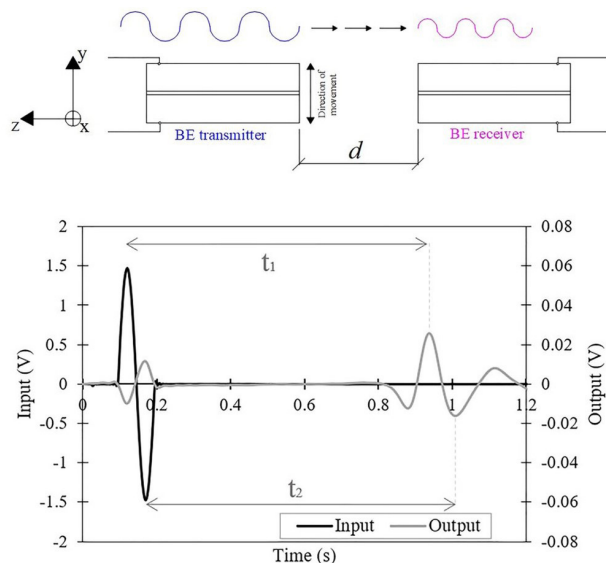


Figure 6. Schematic illustration for determining intervals t_1 e t_2 for the BE3 pair.

After determining the V_s using the relationship of $V_s = d/t$, finally, the maximum shear modulus can be calculated using Equation 3.

G_{max} measurements were performed immediately before each input motion was applied to the base of the box, in order to track the results and map the variation of G_{max} to each input, allowing for a more accurate prediction of model degradation.

5. Shear modulus and damping ratio results

5.1 Shear modulus obtained from resonant column tests

Figure 7 shows the variation of shear modulus over time for the application of each confining stress in the RC tests for the normally consolidated test series. The results of the overconsolidated tests are not shown in this paper as they did not vary much over time, but this issue can be verified in Fernandes (2018).

G_{max} values were obtained by interpolating the last shear modulus measurements to find the modulus relative to 1000 minutes. The G_{max} values for each submitted confining stress are summarized in Table 4, where NC refers to the normally consolidated samples and OC to the overconsolidated ones.

5.2 Shear modulus obtained from centrifuge tests

Figure 8 presents the G modulus for the centrifuge tests, obtained from the accelerometers for model configurations F and C with the respective sinusoidal input amplitudes.

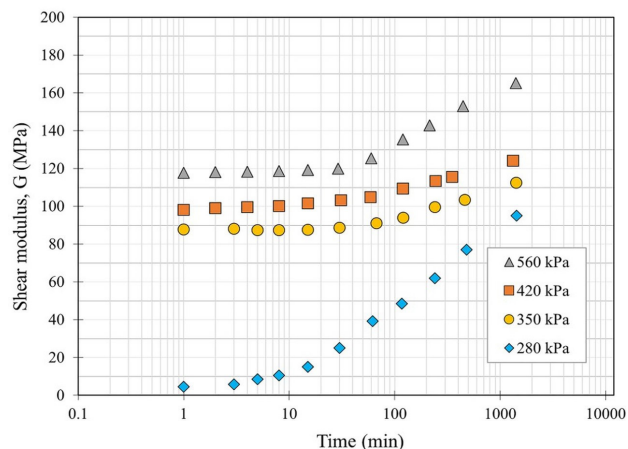


Figure 7. Shear modulus with advancing confined hydrostatic consolidation for the normally consolidated test series (adapted from Fernandes et al., 2020).

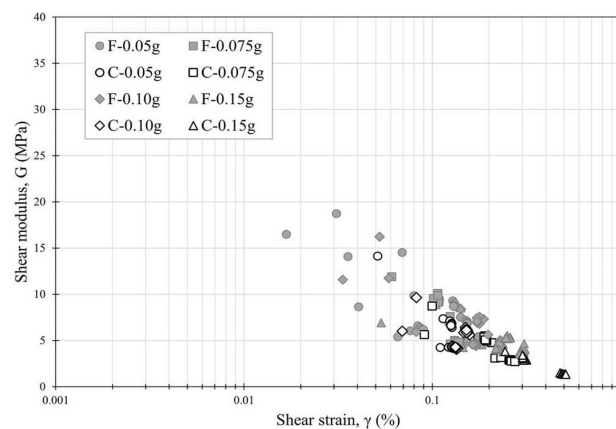


Figure 8. Shear modulus obtained from centrifuge tests.

Table 4. Summary of G_{max} results obtained from RC tests.

Consolidation condition	Confining stress (kPa)	OCR	G_{max} (MPa)
NC	280	1	87
	350	1	108
	420	1	121
	560	1	160
OC	280	2	168
	140	4	120
	70	8	97
	35	16	87

The data points obtained are limited to a strain γ equal to 0.5% but with strains mostly between 0.016% and 0.32%.

Larger values of strains γ are related to larger amplitudes of earthquakes, which are further accentuated in the canyon

model. Furthermore, when F and C models are compared for the same γ , the canyon model produced lower G values, even under lower amplitude loading than the flat model. This is consistent with the fact that the C model suffers from the cumulative effects of excitations as compared to the F model and, therefore, it degrades more. The data points in Figure 8 show the reduction in stiffness and consequent degradation of the shear modulus as seismic loads are applied during the tests.

It is important to note that the depth of the sensor played an important role in the response to shear strain. The deeper accelerometers presented greater shear modulus values for the same strain level, showing the impact of the effective confining stress on the stiffness results.

Table 5 presents the summary of the results of the G_{max} modulus. There is a clear influence of the confinement stress on the velocity results, as the deeper the sensor is, the higher results of V_s and, consequently, of G_{max} . Additionally, for the shallowest sensors (2.6 m and 6.1 m) there is a reduction in the G_{max} values caused by the strength degradation, a degradation that is even greater when comparing the flat and canyon models. As for the deepest sensor (9 m), there was a tendency for G_{max} to increase, caused by the process of consolidation of the model still in progress at this depth.

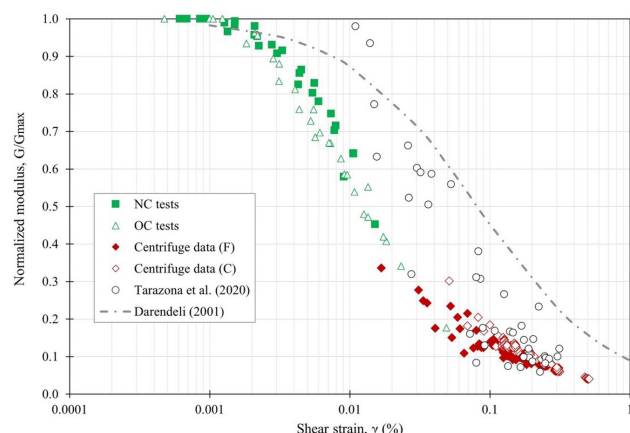


Figure 9. Normalized shear modulus from RC tests, present centrifuge tests, data from Tarazona et al. (2020) and empirical curve of Darendeli (2001).

5.3 Degradation curve by resonant column and centrifuge tests

Several studies have proposed curve models to represent the dynamic behavior of materials (Vucetic & Dobry, 1991; Ishibashi & Zhang, 1993; Darendeli, 2001), but each of these models can reproduce a limited number of behaviors and, therefore, may only be considered as estimates of actual field soil performance (Amir-Faryar et al., 2016).

Darendeli (2001) developed a database of soil samples for the elaboration of empirical curves of normalized shear modulus and damping of materials, which allow the characterization of their dynamic behavior. The data comes from a combination of resonant column and cyclic torsional shear ($RCTS$) tests on undisturbed samples. Statistical analysis was carried out to be able to calibrate the requested parameters, with a structure composed of equations that incorporate the parameters that control the non-linear behavior of the soil, such as overconsolidation ratio, soil plasticity index, mean effective confining stress, type of soil and loading conditions (such as number of cycles and frequency). This model seems to best capture all effects over a wider stress range (Guerreiro et al., 2012).

Figure 9 presents the normalized curve of the modulus G for both phases of confinement of the specimen in the RC tests (NC and OC tests). In addition, it shows the centrifuge results for the F and C models, the data from Tarazona et al. (2020) as well as the empirical curve (EC) from Darendeli (2001) for a material with a plasticity index equal to 39% and considering the average OCR of the model.

As shown in Figure 9, there is low dispersion in the resonant column data associated with strains below 0.01%. It is also observed that the greater the strain, the greater the difference between the G/G_{max} data obtained in the laboratory and the empirical curve. The combined curve formed by RC and centrifuge tests shows a similar trend to the EC , although they deviate significantly from the EC in the strain range between 0.01%–0.1%.

Considering both centrifuge results, those from Tarazona et al. (2020) better adhered to the empirical curve of Darendeli (2001) and are very similar to those of the present study in the range of strains between 0.08% and 0.3%, in which both approach the empirical prediction.

The low adhesion between the laboratory tests and the EC by Darendeli (2001) in some strain ranges can be

Table 5. Summary of G_{max} results obtained through centrifuge tests (in MPa).

Pair of BE	Model	Depth (m)	0.05g	0.75g	0.10g	0.15g
$BE3$	Flat	2.6	23.62	23.07	22.89	22.41
$BE2$		6.1	45.47	44.21	43.72	43
$BE1$		9	65.17	65.33	66.24	66.55
$BE3$	Canyon	2.6	14.7	14.48	14.54	13.35
$BE2$		6.1	31.58	31.29	31.34	28.89
$BE1$		9	-	60.89	-	63.27

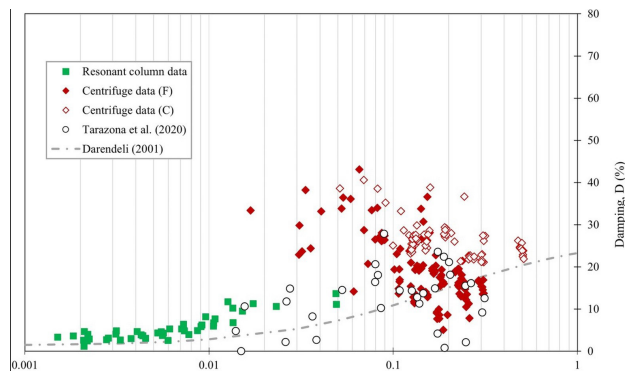


Figure 10. Damping ratio curve with results from resonant column tests, centrifuge tests, Tarazona et al. (2020) data and the Darendeli curve (2001).

explained by the limitation of the model for materials of high plasticity, as is the case of Speswhite kaolin. According to Guerreiro et al. (2012), the model proposed by Darendeli (2001) is quite suitable for materials of medium plasticity, which is not the case of the tested material.

The evolution of the damping ratio results relative to increasing shear strain for all previously analyzed experimental results are shown in Figure 10, along with the Darendeli (2001) curve. The *RC* data shows good agreement with the *EC* from Darendeli (2001). As the strain increases, the average damping data points tend to increase regardless of the method.

For the centrifuge data, the scatter is considerable. This behavior has also been reported by other authors, such as Afacan et al. (2013), Brennan et al. (2005) and Tarazona et al. (2020). Data dispersion is associated with the difficulty in modeling the damping dissipation mechanisms in the context of the centrifuge testing, diverging significantly from the actual damping conditions of the material. Despite this, the data from the *C* model consistently shows greater damping than the data from the *F* model, when subjected to the same strain. This reveals the cumulative effect of the application of dynamic load in reducing the stiffness in the *C* model.

The centrifuge data from the present study and those of Tarazona et al. (2020) present good agreement. Although they are close to Darendeli's (2001) curve, they present data dispersion caused by the centrifuge environment.

6. Conclusions

The present study employed two different methodologies to determine the dynamic parameters of Speswhite kaolin, a material widely used in geotechnical tests. Resonant column and centrifuge tests with *BE* and accelerometers were carried out in parallel to determine the degradation of the shear modulus *G* and the damping curve. These results are presented together with Darendeli's widely used empirical model for the analysis of the non-linear behavior of the soil.

The resonant column and centrifuge tests showed relatively good agreement with those of the empirical curves, both for the degradation of the shear modulus and for the damping ratio at low strains.

Centrifuge tests were effective in evaluating the lower part of the shear modulus degradation curve. For strains above 0.03%, a dispersion of the damping data and its distance from the empirical prediction is noted. This behavior has been reported in the literature and corroborates the difficulty of obtaining this parameter in centrifuge tests. In addition, the poor adherence of the data to the empirical curves in some strain ranges is possibly due to the high plasticity of Speswhite kaolin, an obstacle to the use of the Darendeli curve.

The resonant column tests yielded low dispersion for the shear modulus results and acceptable dispersion for the damping ratio results. The methodology used to carry out the resonant column tests showed yielded low dispersion between the results in the determination of the shear modulus and an acceptable dispersion regarding the damping ratio.

For future studies on this matter, the authors suggest to complement the curves with more data from new *RC* tests with increased consolidation time and new centrifuge tests with strength variation between layers reaching a wider range of strain. Regarding the *BE* results, it is suggested calculation of wave travel time in the frequency domain and the development of numerical studies to validate the presented data.

Acknowledgements

The work described in this article is part of two Cooperation Research Agreements, between PETROBRAS and Federal University of Rio de Janeiro, titled 'Seismic Centrifuge Modelling of Submarine Slopes' and 'Evaluation of Weak Layer on Submarine Landslides' (Contractual Instruments 0050.0094059.14.9 and 5850.0106073.17.9, respectively). The authors thank the staff of the Université Gustave Eiffel and the Institute for Technological Research (IPT) for carrying out the testing program presented in this work, as well as Dr. Sandra Escoffier and Dr. Zheng Li for their insightful recommendations.

Declaration of interest

The authors have no conflicts of interest to declare. All co-authors have observed and affirmed the contents of the paper and there is no financial interest to report.

Authors' contributions

Filipe Cavalcanti Fernandes: Conceptualization, Data curation, Visualization, Writing – original draft. Bárbara Luiza Riz de Moura: Conceptualization, Data curation, Visualization, Writing – original draft & editing. Marcio de

Souza Soares de Almeida: Methodology, Formal analysis, Funding acquisition, Visualization, Writing – review. Luciano de Oliveira Souza Junior: Conceptualization, Data curation, Visualization, Writing – original draft. Samuel Felipe Mollepaza Tarazona: Methodology, Supervision, Visualization. Maria Cascão Ferreira de Almeida: Methodology, Formal analysis, Funding acquisition, Visualization, Writing – review. José Maria de Camargo Barros: Methodology, Supervision, Formal analysis, Writing – review.

Data availability

The datasets generated and analyzed in the course of the current study are available from the corresponding author upon request.

List of symbols

c_v	Coefficient of consolidation
d	Distance between BE of the same pair
m	Exponent to calculate S_u according to Wroth (1984)
n	Parameter to calculate G_{max}/p_r according to Viggiani & Atkinson (1995)
p'	Mean effective stress
p_r	Reference stress (1 kPa)
t_1	Time interval between first peaks of the transmitter and receiver BE
t_2	Time interval between second peaks of the transmitter and receiver BE
t	Average between t_1 and t_2
w_L	Liquid limit
A	Parameter to calculate G_{max}/p_r according to Viggiani & Atkinson (1995)
A_x	Accelerometers with $x = 1, 2, \dots, 22$
BE	Bender elements
C	Canyon (referring to the model configuration)
CR	Resonant column
CAU	Consolidated Anisotropic Undrained
CIU	Consolidated Isotropic Undrained
D	Damping ratio
EC	Empirical curve
ESB	Equivalent shear beam (type of container test)
F	Flat (referring to the model configuration)
G	Shear modulus
G_{max}	Maximum shear modulus
G_s	Specific gravity
I_o	Top inertia + oscillator
I_p	Plasticity index
k	Parameter to calculate G_{max}/p_r according to Viggiani & Atkinson (1995)
K	Normalized strength parameter to calculate S_u according to Wroth (1984)
L	Sample length
NC	Normally consolidated samples

OC	Overconsolidated samples
OCR	Overconsolidation ratio
PGA	Peak ground acceleration
R	Specimen radius
$RCTS$	Cyclic torsional shear
SCPTu	Seismic cone penetration test
SK	Speswhite kaolin
S_u	Undrained strength
TD	Time domain
V_s	Shear wave velocity
γ	Shear strain
θ	Angular rotation
κ	Slope of the isotropic unload-reload line
λ	Slope of the isotropic compression line
M	Critical state friction ratio
ρ	Specific weight
σ'_{vo}	Effective vertical stress
τ	Torsion

References

- Afacan, K.B., Brandenburg, S.J., & Stewart, J.P. (2013). Centrifuge modeling studies of site response in soft clay over wide strain range. *Journal of Geotechnical and Geoenvironmental Engineering*, 140(2), 04013003. [https://10.1061/\(asce\)gt.1943-5606.0001014](https://10.1061/(asce)gt.1943-5606.0001014).
- Almeida, M.S.S., Davies, M.C.R., & Parry, R.H.G. (1985). Centrifuged embankments on strengthened and unstrengthened clay foundations. *Geotechnique*, 35(4), 425-441. <http://dx.doi.org/10.1680/geot.1985.35.4.425>.
- Al-Tabbaa, A. (1987). *Permeability and stress-strain response of Speswhite kaolin* [Doctoral thesis]. Cambridge University.
- Amir-Faryar, B., Aggour, M.S., & McCuen, R.H. (2016). Universal model forms for predicting the shear modulus and material damping of soils. *Geomechanics and Geoengineering*, 12(1), 60-71. <http://dx.doi.org/10.1080/17486025.2016.1162332>.
- Anderson, D.G., & Stokoe, K.H. (1978). Shear modulus: a time-dependent soil property. In R. J. Ebelhar, V. P. Drnevich & B. L. Kutter (Eds.), *Dynamic geotechnical testing* (pp. 66-90). ASTM. <https://doi:10.1520/STP35672S>.
- ASTM D4015-07. (2007). *Standard test methods for modulus and damping of soils by resonant-column method*. ASTM International, West Conshohocken, PA. <https://doi.org/10.1520/D4015-07>.
- Atkinson, J.H. (2007). *The mechanics of soils and foundations* (2nd ed.). Taylor & Francis.
- Barros, J.M.C., Silveira, R.M.S., & Amaral, C.S. (2007). Correlation between the maximum shear modulus and the undrained strength of a remolded marine clay. In *Proc. XIII Panamerican Conference on Soil Mechanics and Geotechnical Engineering* (pp. 514-519). Isla de Margarita, Venezuela. Sociedad Venezolana de Geotecnia.
- Borges, R.G., Assumpção, M.S., Almeida, M.C.F., & Almeida, M.S.S. (2020a). Seismicity and seismic hazard in the

- continental margin of southeastern Brazil. *Journal of Seismology*, 24(6), 1205-1224. <http://dx.doi.org/10.1007/s10950-020-09941-4>.
- Borges, R.G., Souza Junior, L.O., Almeida, M.C.F., & Almeida, M.S.S. (2020b). Relationship between shear wave velocity and piezocone penetration tests on the Brazilian continental margin. *Soils and Rocks*, 43, 219-230. <http://dx.doi.org/10.28927/SR.432219>.
- Brennan, A.J., Thusyanthan, N.I., & Madabhushi, S.P.G. (2005). Evaluation of shear modulus and damping in dynamic centrifuge tests. *Journal of Geotechnical and Geoenvironmental Engineering*, 131(12), 1488-1497. [http://dx.doi.org/10.1061/\(ASCE\)1090-0241\(2005\)131:12\(1488\)](http://dx.doi.org/10.1061/(ASCE)1090-0241(2005)131:12(1488)).
- Darendeli, M.B. (2001). *Development of a new family of normalized modulus* [Doctoral dissertation, University of Texas at Austin]. University of Texas at Austin's repository. Retrieved in December 3, 2022, from <http://hdl.handle.net/2152/10396>
- Fernandes, F.C. (2018). *Resonant column and bender element tests with Speswhite kaolin for shear modulus measurement* [Master's dissertation, Federal University of Rio de Janeiro]. Federal University of Rio de Janeiro's repository (in Portuguese). Retrieved in December 3, 2022, from <http://hdl.handle.net/11422/11402>.
- Fernandes, F.C., Tarazona, S.F.M., Almeida, M.C.F., Almeida, M.S.S., & Barros, J.M.C. (2020). Ensaaios de coluna ressonante em caulim Speswhite. In *Proc. XX Congresso Brasileiro de Mecânica dos Solos e Engenharia Geotécnica* (pp. 1-8). Campinas. Retrieved in December 3, 2022, from <https://proceedings.science/cobramseg-2022/trabalhos/ensaaios-de-coluna-ressonante-em-caulim-speswhite?lang=pt-br>. (in Portuguese).
- Garala, T.K., & Madabhushi, G.S. (2019). Seismic behaviour of soft clay and its influence on the response of friction pile foundations. *Bulletin of Earthquake Engineering*, 17(4), 1919-1939. <http://dx.doi.org/10.1007/s10518-018-0508-4>.
- Garnier, J. (2001). Modèles physiques en géotechnique. *Revue Française de Géotechnique*, 97, 3-29. <http://dx.doi.org/10.1051/geotech/2001097003>.
- Guerreiro, P., Kontoe, S., & Taborada, D. (2012). Comparative study of stiffness reduction and damping curves. In *Proc. 15th World Conference on Earthquake Engineering* (pp. 2-11). Lisbon. SPES.
- Hall, J., & Richart, F.E. (1963). Dissipation of elastic wave energy in granular soils. *Journal of the Soil Mechanics and Foundations Division*, 89(6), 27-56. <http://dx.doi.org/10.1061/JSFEAQ.0000568>.
- Hardin, B.O., & Drnevich, V.P. (1972). Shear modulus and damping in soils: design equations and curves. *Journal of the Soil Mechanics and Foundations Division*, 98(7), 667-692. <http://dx.doi.org/10.1061/JSFEAQ.0001760>.
- Ingale, R., Patel, A., & Mandal, A. (2017). Performance analysis of piezoceramic elements in soil: a review. *Sensors and Actuators. A, Physical*, 262, 46-63. <http://dx.doi.org/10.1016/j.sna.2017.05.025>.
- Ishibashi, I., & Zhang, X. (1993). Unified dynamic shear moduli and damping ratios of sand and clay. *Soils and Foundations*, 33(1), 182-191. <https://10.3208/sandf1972.33.182>.
- Jafari, S.H., Lajevardi, S.H., & Sharifipour, M. (2022). Correlation between small-strain dynamic properties and unconfined compressive strength of lime-stabilized soft clay. *Soil Mechanics and Foundation Engineering*, 59(4), 331-337. <http://dx.doi.org/10.1007/s11204-022-09819-2>.
- Jia, J. (2018). *Soil dynamics and foundation modeling*. Springer. <https://doi:10.1007/978-3-319-40358-8>.
- Kondner, R.L. (1963). Hyperbolic stress-strain response: cohesive soils. *Journal of the Soil Mechanics and Foundations Division*, 89(1), 115-143. <http://dx.doi.org/10.1061/JSFEAQ.0000479>.
- Kowsmann, R.O., Falcão, A.P.C., & Curbelo-Fernandez, M.P. (2015). *Geologia e geomorfologia*. Elsevier (in Portuguese).
- Kutter, B., & James, R. (1989). Dynamic centrifuge model tests on clay embankments. *Geotechnique*, 39(1), 91-106. <http://dx.doi.org/10.1680/geot.1989.39.1.91>.
- Lang, L., Li, F., & Chen, B. (2020). Small-strain dynamic properties of silty clay stabilized by cement and fly ash. *Construction & Building Materials*, 237, 117646. <http://dx.doi.org/10.1016/j.conbuildmat.2019.117646>.
- Lee, J.-S., & Santamarina, C. (2005). Bender elements: performance and signal interpretation. *Journal of Geotechnical and Geoenvironmental Engineering*, 131(9), 1063-1070. [http://dx.doi.org/10.1061/\(asce\)1090-0241\(2005\)131:9\(1063\)](http://dx.doi.org/10.1061/(asce)1090-0241(2005)131:9(1063)).
- Liu, Z., Kim, J., Hu, G., Hu, W., & Ning, F. (2021). Geomechanical property evolution of hydrate-bearing sediments under dynamics loads: nonlinear behaviors of modulus and damping ratio. *Engineering Geology*, 295, 106427. <http://dx.doi.org/10.1016/j.enggeo.2021.106427>.
- Madhusudhan, B.N., & Kumar, J. (2013). Damping of sands for varying saturation. *Journal of Geotechnical and Geoenvironmental Engineering*, 139(9), 1625-1630. [http://dx.doi.org/10.1061/\(ASCE\)GT.1943-5606.0000895](http://dx.doi.org/10.1061/(ASCE)GT.1943-5606.0000895).
- Mair, R.J. (1993). Developments in geotechnical engineering research: application to tunnels and deep excavation. *Proceedings of the Institution of Civil Engineers. Civil Engineering*, 93, 27-41.
- Mérindol, M., St-Onge, G., Sultan, N., Lajeunesse, P., & Garziglia, S. (2022). Earthquake-triggered submarine landslides in the St. Lawrence Estuary (Québec, Canada) during the last two millennia and the record of the major 1663 CE M \geq 7 event. *Quaternary Science Reviews*, 291(1), 107640. <http://dx.doi.org/10.1016/j.quascirev.2022.107640>.
- Phillips, N. (1988). *Centrifuge lateral pile tests in clay: tasks 2 and 3: a report by Exxon Production Research Corp.* Lynxvale Ltd.

- Randolph, M.F., & Houlsby, G.T. (1984). The limiting pressure on a circular pile loaded laterally in cohesive soil. *Geotechnique*, 34(4), 613-623. <http://dx.doi.org/10.1680/geot.1984.34.4.613>.
- Richart, F.E., Hall, J.R., & Woods, R.D. (1970). *Vibrations of soils and foundations*. Prentice-Hall.
- Soriano, C., Almeida, M.C.F., Almeida, M.S.S., Madabhushi, G.S., & Stanier, S. (2022). Centrifuge modeling of the seismic behavior of soft clay slopes. *Journal of Geotechnical and Geoenvironmental Engineering*, 148(11), 04022089. [http://dx.doi.org/10.1061/\(ASCE\)GT.1943-5606.0002884](http://dx.doi.org/10.1061/(ASCE)GT.1943-5606.0002884).
- Soriano, C., Almeida, M.C.F., Madabhushi, S.P.G., Stanier, S.A., Almeida, M.S.S., Liu, H., & Borges, R.G. (2021). Seismic centrifuge modeling of a gentle slope of layered clay, including a weak layer. *Geotechnical Testing Journal*, 45(1), 125-144. <http://dx.doi.org/10.1520/GTJ20200236>.
- Souza, L.O. (2021). *Centrifuge modeling of submarine slopes subjected to seismic movements* [Master's dissertation, Federal University of Rio de Janeiro]. Federal University of Rio de Janeiro's repository.
- Tarazona, S.F.M. (2019). *Evaluation of seismic site response of submarine clay canyons* [Doctoral thesis, Federal University of Rio de Janeiro]. Federal University of Rio de Janeiro's repository.
- Tarazona, S.F.M., Almeida, M.C.F., Bretschneider, A., Almeida, M.S.S., Escoffier, S., & Borges, R.G. (2020). Evaluation of seismic site response of submarine clay canyons using centrifuge modelling. *International Journal of Physical Modelling in Geotechnics*, 20(4), 224-238. <https://doi.10.1680/jphmg.18.00084>.
- Viggiani, G., & Atkinson, J. (1995). Stiffness of fine-grained soil at very small strains. *Geotechnique*, 45(2), 249-265. <http://dx.doi.org/10.1680/geot.1995.45.2.249>.
- Vucetic, M., & Dobry, R. (1991). Effect of soil plasticity on cyclic response. *Journal of Geotechnical Engineering*, 117(1), 89-107. [http://dx.doi.org/10.1061/\(ASCE\)0733-9410\(1991\)117:1\(89\)](http://dx.doi.org/10.1061/(ASCE)0733-9410(1991)117:1(89)).
- Wang, F., Li, D., Du, W., Zarei, C., & Liu, Y. (2021). Bender element measurement for small-strain shear modulus of compacted loess. *International Journal of Geomechanics*, 21(5), 04021063. [http://dx.doi.org/10.1061/\(asce\)gm.1943-5622.0002004](http://dx.doi.org/10.1061/(asce)gm.1943-5622.0002004).
- Wroth, C.P. (1984). The interpretation of in situ soil tests. *Geotechnique*, 34(4), 449-489. <http://dx.doi.org/10.1680/geot.1984.34.4.449>.
- Youn, J.U., Choo, Y.W., & Kim, D.S. (2008). Measurement of small-strain shear modulus G_{max} of dry and saturated sands by bender element, resonant column, and torsional shear tests. *Canadian Geotechnical Journal*, 45(10), 1426-1438. <http://dx.doi.org/10.1139/T08-069>.
- Zhang, L., Goh, S.H., & Yi, J. (2016). A centrifuge study of the seismic response of pile-raft systems embedded in soft clay. *Geotechnique*, 67(6), 479-490. <http://dx.doi.org/10.1680/jgeot.15.p.099>.